Minimum variability time-scales of long and short GRBs

G. A. MacLachlan,[1]⋆ A. Shenoy,[1] E. Sonbas,[2,3] K. S. Dhuga,[1] B. E. Cobb,[1]
T. N. Ukwatta,[1,3,4] D. C. Morris,[1,3,5] A. Eskandarian,[1] L. C. Maximon[1]
and W. C. Parke[1]

[1]*Department of Physics, The George Washington University, Washington, DC 20052, USA*
[2]*Department of Physics, University of Adiyaman, 02040 Adiyaman, Turkey*
[3]*NASA Goddard Space Flight Center, Greenbelt MD 20771, USA*
[4]*Department of Physics and Astronomy, Michigan State University, East Lansing MI 48824, USA*
[5]*Department of Physics, University of Virgin Islands, Virgin Islands, USA*

ABSTRACT

We have investigated the time variations in the light curves from a sample of long and
short *Fermi*/GBM gamma-ray bursts (GRBs) using an impartial wavelet analysis. The results
indicate that in the source frame, the variability time-scales for long bursts differ from that
for short bursts, variabilities of the order of a few milliseconds are not uncommon and an
intriguing relationship exists between the minimum variability time and the burst duration.

Key words: methods: analytical – methods: data analysis – methods: statistical – gamma-ray
burst: general.

1 INTRODUCTION

The prompt emission from gamma-ray bursts (GRBs) shows complex time profiles that have eluded a generally accepted explanation. Fenimore & Ramirez-Ruiz (2000) reported a correlation between variability of GRBs and the peak isotropic luminosity. The existence of the variability–luminosity correlation suggests that the prompt emission light curves have embedded temporal information related to the microphysics of GRBs. Several models have been proposed to explain the observed temporal variability of GRB light curves. Leading models such as the internal shock model (Kobayashi, Piran & Sari 1997) and the photospheric model (Ryde 2004) link the rapid variability directly to the activity of the central engine. Others invoke relativistic outflow mechanisms to suggest that local turbulence amplified through Lorentz boosting leads to causally disconnected regions which in turn act as independent centres for the observed prompt emission. Within more recent models, Morsony, Lazzati & Begelman (2010) and Zhang & Yan (2011) argue that the temporal variability may show two different scales depending on the physical mechanisms generating the prompt emission.

In order to further our understanding of the prompt emission phase of GRBs and to explicitly test some of the key ingredients in the various models, it is clearly important to extract the variability for both short and long GRBs in a robust and unbiased manner. It is also clear that the chosen methodology should not only be mathematically rigorous but also be sufficiently flexible to apply to transient phenomena with multiple time-scales and a wide dynamic range. A wide dynamic range is naturally provided by the bimodal separation of GRB duration occurring at $T_{90} = 2$ s as observed by Kouveliotou et al. (1993) to distinguish between long- and short-duration GRBs.

In this paper, we extract variability time-scales for GRBs using a method based on wavelets. The technique for such a temporal analysis is universal and has the advantage over Fourier analysis that transients and frequency correlations can be more easily picked out in the data. Results presented herein were compared with Bhat et al. (2012), who gave pulse parameters for approximately 400 pulses obtained from 34 GRBs. It was shown by MacLachlan et al. (2012) that the minimum variability time-scale tracks the rise times of pulses very well for over three orders of magnitude in time-scale. The relation of minimum variability time-scales to pulse parameters has been extended to four orders of magnitude by Sonbas et al. (2012), who applied the present technique to analyse X-ray flares.

The time-scales being investigated here have power densities very near to that of the noise in the data which makes extracting these time-scales non-trivial. A somewhat older but still interesting discussion of extracting signal in a noisy environment can be found in Scargle (1982) and a more recent discussion found in Kostelich & Schreiber (1993). The technique we offer is not necessarily new but is different from previous published wavelet analyses (Fritz & Bruch 1998; Walker, Schaefer & Fenimore 2000; Tamburini, De Martino & Bianchini 2009; Anzolin et al. 2010)[1] in that we apply a number of modifications suggested by various authors (Coifman & Donoho 1995; Strang & Nguyen 1997; Percival & Walden 2000; Addison 2002) as explained further in Section 4.

---

[1] Note that Fritz & Bruch (1998) analysed optical data and Tamburini et al. (2009) and Anzolin et al. (2010) X-ray data from cataclysmic variables.

⋆ E-mail: maclach@gwu.edu

The layout of the paper is as follows: the source of the data is described in Section 2; the main aspects of the wavelet methodology are outlined in Section 3; in Section 4, we provide the details of the data analysis; in Section 5, we present and discuss our main findings; finally, in Section 6, we summarize our conclusions.

2 DATA

The Gamma-Ray Burst Monitor (GBM) on board *Fermi* observes GRBs in the energy range 8 keV to 40 MeV. The GBM is composed of 12 thallium-activated sodium iodide (NaI) scintillation detectors (12.7 cm in diameter by 1.27 cm thick) that are sensitive to energies in the range of 8 keV to 1 MeV, and two bismuth germanate (BGO) scintillation detectors (12.7 cm diameter by 12.7 cm thick) with energy coverage between 200 keV and 40 MeV. The GBM detectors are arranged in such a way that they provide a significant view of the sky (Meegan et al. 2009).

In this work, we have extracted light curves for the GBM NaI detectors over the entire energy range (8 keV to 1 MeV, also including the overflow beyond 1 MeV). Typically, the brightest three NaI detectors were chosen for the extraction. Light curves for both long and short GRBs were extracted at a time binning of 200 μs. The long GRBs were extracted over a duration starting from 20 s before the trigger and up to about 50 s after the T_{90} for the burst without any background subtraction. For short GRBs, durations were chosen to be 20 s before the trigger and 10 s after the T_{90}. The T_{90} durations were obtained from the *Fermi* GBM-Burst Catalogue (Paciesas et al. 2012).

3 METHODOLOGY

We report on our model-independent statistical investigation of the variability of *Fermi*/GBM long and short GRBs. We extract this information by using a fast wavelet transformation to encode GRB light curves into a wavelet representation and then compute a statistical measure of the variance of wavelet coefficients over multiple time-scales.

3.1 Minimum variability time-scales

It is often the case when multiple processes are present that one process will dominate the others at certain time-scales but those same processes may exchange dominance at other time-scales. A wavelet technique is useful in these situations because the variances of wavelet coefficients are sensitive to whichever processes dominate the light curve at a given time-scale. Moreover, the technique can be used to classify those dominant processes as well as provide a means to determine the characteristic time-scale, τ_β, for which the processes exchange dominance. Determination of τ_β helps in the development of theoretical models and the understanding of observational data. Indeed, if there is a transition from a time-scaling region to that of white noise, then there is a smallest variability time for the physical processes present.

3.2 Wavelet transforms

Wavelet transformations have been shown to be a natural tool for the multiresolution analysis of non-stationary time series (Flandrin 1989, 1992; Mallat 1989). Wavelet analysis is similar to Fourier analysis in many respects but differs in that wavelet basis functions are well localized, i.e. have compact support, while Fourier basis

functions are global. Compact support means that outside some finite range the amplitude of wavelet basis functions goes to zero or is otherwise negligibly small (Percival & Walden 2000). In principle, a wavelet expansion forms a faithful representation of the original data, in that the basis set is orthonormal and complete.

3.2.1 Discrete dyadic wavelet transforms

Given the discrete nature of the data, we employ a discrete wavelet analysis. The rescaled translated nature of the wavelet basis functions makes the wavelet transform well localized in both frequency and time, which results in an insensitivity to background photon counts expressed by polynomial fits. The level of insensitivity, formally known as the vanishing moment condition, can be adjusted by the choice of the wavelet basis function. By construction, the discrete wavelet transform is a multiresolution operation (Mallat 1989). Such wavelets, denoted as $\psi_{j,k}(t)$, form a dyadic basis set, i.e. wavelets in the set have variable widths and variable central time positions.

The wavelet analysis employed in this study, as with the fast Fourier transform, begins with a light curve with N elements,

$$X_i = \{X_0 \ldots X_{N-1}\}, \tag{1}$$

where N is an integer power of 2. The light curve is convolved with a scaling function, $\phi_{j,k}(t_i)$, and wavelet function, $\psi_{j,k}(t_i)$, which are rescaled and translated versions of the original scaling and wavelet functions $\phi(t_i) = \phi_{0,0}$ and $\psi(t_i) = \psi_{0,0}$. Translation is indexed by k and rescaling is indexed by j. The rescaling and translation relation is given by

$$\psi_{j,k}(t) = 2^{-j/2} \psi(2^{-j}t - k). \tag{2}$$

The precise forms of the scaling and wavelet functions are not unique. The choices are made according to the features one wishes to exploit (Percival & Walden 2000; Addison 2002). The scaling function acts as a smoothing filter for the input time series and the wavelet function probes the time series for detail information at some time-scale, Δt, which is twice that of the finest binning of the data, T_{bin}. In the analysis, the time-scale is doubled

$$\Delta t \to 2\Delta t$$

and the transform is repeated until

$$\Delta t = NT_{\mathrm{bin}}.$$

In this analysis, we choose the Haar (Addison 2002) scaling/wavelet basis because it has the smallest possible support, has one vanishing moment and is equivalent to the Allan variance (Howe & Percival 1995), allowing for a straightforward interpretation.

3.2.2 The Haar wavelet basis

Convolving the light curve, X, with the scaling functions yields approximation coefficients,

$$a_{j,k} = \langle \phi_{j,k}, X \rangle. \tag{3}$$

Interrogating X with the wavelet basis functions yields scale- and position-dependent detail coefficients,

$$d_{j,k} = \langle \psi_{j,k}, X \rangle. \tag{4}$$

It is interesting to point out that for the trivial $N = 2$ case, the Haar wavelet transform and the Fourier transform are identical.

3.3 Log-scale diagrams and scaling

Log-scale diagrams are useful for identifying scaling and noise regions. Construction of a log-scale diagram for each GRB proceeds from the variance of detail coefficients (Flandrin 1992),

$$\beta_j = \frac{1}{n_j} \sum_{k=0}^{n_j-1} |d_{j,k}|^2, \tag{5}$$

where the n_j are the number of detail coefficients at a particular scale, j. A plot of $\log_2$ variances versus scale, j, takes the general form

$$\log_2 \beta_j = \alpha j + \text{constant}, \tag{6}$$

and is known as a log-scale diagram. A linear regression is made of each log-scale diagram and the slope parameter, α (depicting a measure of scaling), is estimated. White-noise processes appear in log-scale diagrams as flat regions while non-stationary processes appear as sloped regions with the following condition on the slope parameter, $\alpha > 1$ (Flandrin 1989; Percival & Walden 2000; Abry et al. 2003).

4 DATA ANALYSIS

4.1 Background subtraction

We now present a method for removing photometric background due to noise not intrinsic to the GRB so that physical variability arising from the GRB remains for further analysis. Background subtraction for a statistical analysis of variability via wavelet transforms should proceed in the space variances as opposed to a traditional flat or linear subtraction of counts. This owes to the fact that Haar detail coefficients are insensitive to polynomial trends in the signal up to first order. Subtraction of a flat or linear background from a light curve is an operation under which the wavelet transform is invariant (as are Fourier transforms) apart from the mean signal coefficient.

The GRB light curves show power at various variability time-scales. Most often, there is a region of the log-scale diagram (log-power verses log-variability time) with a single slope, indicating scaling in the power over those variability times, and a flat region at the shortest variability times, indicating the presence of white noise. Some of this white noise may be intrinsic to the GRB. Some may be attributed to instrumental noise and to background emissions from sources not including the GRB in question. We therefore express the variability of the burst, β_j^{burst}, at time-scales j as comprising of individual variances: a scaling component, β^{scaling}; an intrinsic noise component, β^{noise}, and a background component, $\beta^{\text{background}}$. The variability of the burst can then be described as a linear combination of the component variances so long as the components have vanishing covariances. In this event we write

$$\beta_j^{\text{burst}} = \beta_j^{\text{scaling}} + \beta_j^{\text{noise}} + \beta_j^{\text{background}}. \tag{7}$$

The minimum variability time-scale, τ_β, is identified from a log-scale diagram by the octave, $j_{\text{intersection}}$, of the intersection of the flat intrinsic noise domain, β_j^{noise}, with the sloped scaling domain, β_j^{scaling},

$$\tau_\beta \equiv T_{\text{bin}} \times 2^{j_{\text{intersection}}}. \tag{8}$$

In practice, the octave at which the intersection occurs is determined by equating the polynomial fits to the flat intrinsic noise domain and the sloped scaling domain and solving for $j_{\text{intersection}}$. The uncertainty in τ_β is determined by propagating the uncertainty in the parameters
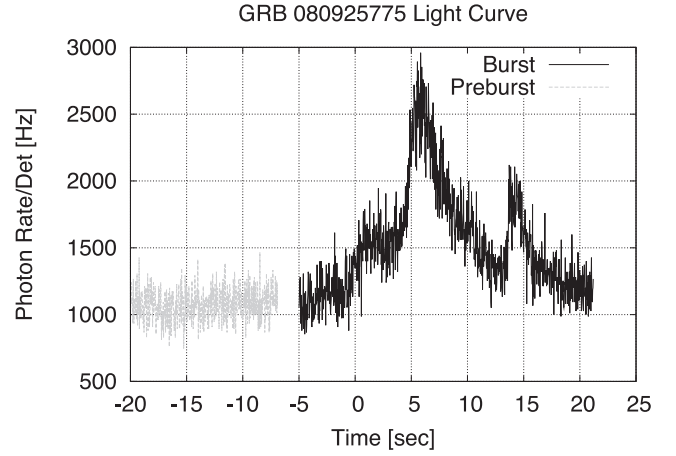

Figure 1. GBM GRB080925775. Preburst portion of the light curve, used for background removal, is shown in grey. The burst portion, from which a time-scale is extracted, is shown in black.

from the fits to the β_j which in turn follow from a bootstrap procedure described in Sections 4.1.2 and 4.1.3. It is at this time-scale, τ_β, that a structured physical process appears to give way to one that is stochastic and unstructured. Clearly one seeks to remove $\beta_j^{\text{background}}$ from equation (7) to arrive at the cleanest possible signal,

$$\beta_j^{\text{burst}} \to \beta_j^{\text{clean}} \equiv \beta_j^{\text{burst}} - \beta_j^{\text{background}} = \beta_j^{\text{scaling}} + \beta_j^{\text{noise}}. \tag{9}$$

In order to estimate the variance of the background during the burst, we will assume that the variance obtained from a preburst portion of the light curve can serve as an acceptable surrogate for the background variance. That is,

$$\beta_j^{\text{preburst}} \equiv \beta_j^{\text{background}}, \tag{10}$$

and then the background is removed from the signal according to the relation

$$\log_2(\beta_j^{\text{clean}}) = \log_2(\beta_j^{\text{burst}} - \beta_j^{\text{preburst}}). \tag{11}$$

A simple algebraic manipulation of equation (11) gives a form,

$$\log_2(\beta_j^{\text{clean}}) = \log_2(\beta_j^{\text{burst}}) + \log_2\left(1 - \frac{\beta_j^{\text{preburst}}}{\beta_j^{\text{burst}}}\right). \tag{12}$$

For long GRBs, the preburst is defined relative to a zero-second trigger time as T-20 s to T-5 s and for short GRBs the preburst is defined to be from T-15 s to T-1 s. Here T is the trigger time of the burst (see Fig. 1).

4.1.1 Statistical uncertainties

We have considered the statistical uncertainties in the light curve by a typical bootstrap approach in which the square root of the number of counts per bin is used to generate an additive Poisson noise. A new Poisson noise is considered for each iteration through the bootstrap process. More significant contributions to the uncertainties are discussed in Sections 4.1.2 and 4.1.3.

4.1.2 Circular permutation

Spurious artefacts due to incidental symmetries resulting from accidental misalignment (Coifman & Donoho 1995; Percival & Walden 2000) of light curves with wavelet basis functions are minimized by

circularly shifting the light curve against the basis functions. Circular shifting is a form of translation invariant de-noising (Coifman & Donoho 1995). It is possible that a shift will introduce additional artefacts by moving a different symmetry into a susceptible location. Thus, our approach is to circulate the signal through all possible values, or at least a representative sampling, and then take an average over the cases which do not show spurious correlations.

4.1.3 Reverse-tail concatenation

Both discrete Fourier and discrete wavelet transformations imply an overall periodicity equal to the full time range of the input data. This can be interpreted to mean that for a series of N elements, $\{X_0, X_1 \ldots X_{N-1}\}$, then X_0 is made a surrogate for X_N, X_1 is made a surrogate for X_{N+1}, and so forth. This assumption may lead to trouble if X_0 is much different from X_{N-1}. In this case, artificially large variances may be computed. Reverse-tail concatenation minimizes this problem by making a copy of the series which is then reversed and concatenated on to the end of the original series resulting in a new series with a length twice that of the original. Instead of matching boundary conditions like

$$X_0, X_1, \ldots, X_{N-1}, X_0, \tag{13}$$

we match boundaries as

$$X_0, X_1, \ldots X_{N-1}, X_{N-1}, \ldots, X_1, X_0. \tag{14}$$

Note that the series length has thus artificially been increased to $2N$ by reversing and doubling of the original series. Consequently, the wavelet variances at the largest scale in a log-scale diagram reflect this redundancy. This is the reason why the wavelet variances at the largest scale are excluded from least-squares fits of the scaling region.

Another difficulty in wavelet expansions is that the initialization procedure of the multiresolution algorithm may pollute the detail coefficients at the finest scale (see Strang & Nguyen 1997; Abry et al. 2003). For this reason, we follow the advice of Abry et al. (2003) and discard the detail coefficients at the finest scale.

4.2 Simulation

The efficacy of this background subtraction method and the sensitivity to signal to noise was tested using simulated data in the form of fractional Brownian motion (fBm) time series that were first discussed by Mandelbrot & Van Ness (1968). One advantage of using fBms for simulation of time series data is that short duration, statistically significant fluctuations which trigger the identification of a minimum variability time-scale arise naturally as part of the random process which produces them. Another is that fBms have a scaling parameter, α, which is easily varied.

The outline of the simulation procedure begins with using the numerical computing environment MATLAB to produce 1000 realizations of fBms with scaling parameter α randomly chosen from the range $1.0 \leq \alpha \leq 2.0$ by using a uniform random number generator. The fBms were then acted upon by a Poisson operator which transformed each time series into a Poisson-distributed series but left other properties of the fBm intact, e.g. α.

The fBms were then combined with a Poisson noise with variance, λ_B. These Poisson noises were regarded as intrinsic to the GRB. Another set of Poisson noises with variances, λ_I, were generated and these noise signals were interpreted as external *background* meant to be removed by the subtraction procedure.
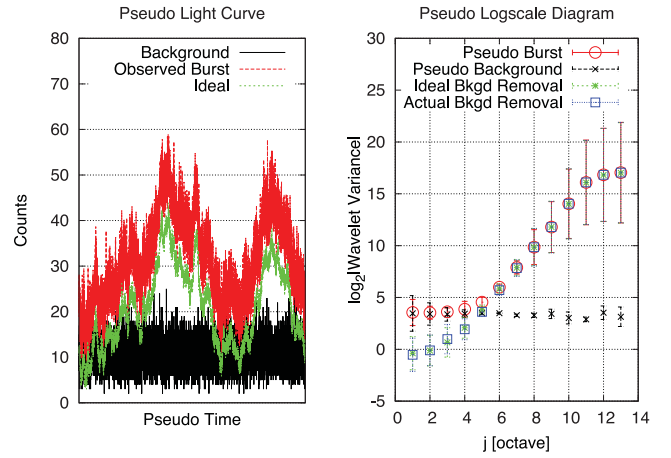

Figure 2. In the left-hand panel are simulated light curves and noise processes: an *ideal* fBm process (green) and a *background* Poisson noise (black). The sum of the fBm and Poisson processes is shown in red and is labelled *observed*. The *observed* light curve (red) is the sum of the fBm and Poisson noise. The right-hand panel shows the results of the background subtraction procedure. The red and black points show the log-scale diagrams corresponding to the *observed* light curve and *background*, respectively. The green data show the log-scale diagram for the *ideal* light curve and the blue data are the log scale with background removed. The agreement between green and blue data demonstrates the merit of the background removal procedure.

The idealized light curves were then combined with external backgrounds resulting in pseudo-*observed* light curves shown in red in the left-hand panel of Fig. 2. The pseudo-observed light curves and the external background noises were transformed into wavelet coefficients and wavelet variances were computed according to equation (5). The variances of the pseudo-observed light curve (labelled *actual*) and the background are plotted in the right-hand panel of Fig. 2 in red and black, respectively. The background was subtracted from the pseudo-observed light curve as detailed in equation (12), and the resulting corrected variances are plotted in blue in the right-hand panel of Fig. 2. The corrected variances are to be compared to the variances of the ideal light curve which are plotted in green.

4.2.1 Signal-to-noise sensitivity

We define a brightness parameter, ξ, such that

$$\xi \equiv 2^{\delta/2}, \tag{15}$$

where

$$\delta \equiv \log_2 \lambda_B - \log_2 \lambda_I. \tag{16}$$

Ideally the octave, $j_{\text{intersection}}$, which is related to the minimum variability time-scale, τ_β, as defined in equation (8) is completely determined by ξ, λ_I, α, and the standard deviation of the increments of the fBm, σ. We fixed the values of λ, σ and varied α and ξ so that the expected values of $j_{\text{intersection}}$ are $\langle j_{\text{intersection}} \rangle = \{6, 7\}$. The time series thus produced were then analysed as described in Section 4.1. The results of the simulation are given in Fig. 3. The horizontal red and blue lines show the expected $j_{\text{intersection}}$ for octaves 6 and 7, respectively, and are given as a guide. Brightness, ξ, increases to the right. We show in grey the region along the ξ-axis, where we find the GRBs analysed in this paper based on the background noise level and the estimated noise level intrinsic to the GRB. We
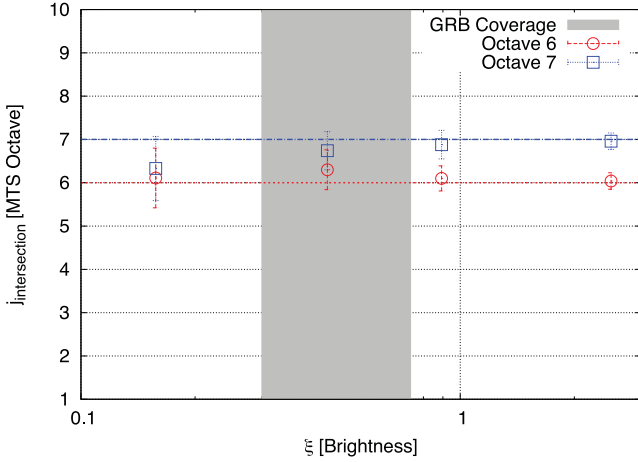
Figure 3. Results of signal-to-noise sensitivity test. We generated 1000 simulated light curves with expected $j_{\text{intersection}}$ equal to 6 and 7 for various brightness. We show in grey the region along the ξ-axis, where we find the GRBs analysed in this paper, $0.3 < \xi < 0.74$. We note that in the region covered by the GRBs presented herein, brightness does not affect $j_{\text{intersection}}$ greatly.

have noted by our own experience that for $\xi < 0.1$, the technique discussed in this paper performs poorly. However, in the range of signal to noise sampled by the GRBs used here, $0.3 < \xi < 0.74$, the background subtraction technique does not suffer from a large systematic response to variations in brightness, as can be seen in Fig. 3.

4.2.2 Flux sensitivity

We also investigated the reliability of the analysis as a function of flux by removing randomly selected counts from the original simulated signal component while leaving the background noise level undisturbed. The analysis is then repeated for the newly *dimmed* simulated light curves and comparison is made to the original un-dimmed version. This brightness comparison is similar to the one described in Norris et al. (1995) but with a different normalization. In Norris et al. (1995) light curves were normalized by peak intensities. In this study, the simulated light curves were normalized by signal power at the time-scales specified by the dyadic partitioning of the wavelet transform.

Dimming of the simulated light curves was done by removing 0–10 per cent and reanalysing then repeating by removing 10–20 per cent and so forth up to 70–80 per cent. We also considered the effect of larger variations in count removal, i.e. removing 0–25 per cent, 25–50 per cent and 50–75 per cent. We find that a decrease in flux has essentially the same effect on τ_β as increasing the noise level. However, the largest effect was by the wider bite of counts. For example, one can expect more accurate results from this analysis by removing 30–40 per cent of counts on a bin to bin basis than by removing 25–50 per cent. We conclude that flux-related effects are more serious when it varies widely throughout the duration of the light curve. In all cases, we have studied removing 80 per cent or more of the counts in the signal was a reliable way to make the method fail. Fortunately, when the method fails in this way it does so in an obvious way, i.e. the white-noise signal power coefficients in the log-scale diagram become highly irregular. As discussed in Section 4.3, we test for this effect in the GRB data by performing

Table 1. Short GRBs (observer frame).

GRB	T_{90} (s)	δT_{90} (s)	τ_β (s)	$\delta\tau_\beta^-$ (s)	$\delta\tau_\beta^+$ (s)
080723913	0.192	0.345	0.0307	0.0192	0.0510
081012045	1.216	1.748	0.0052	0.0024	0.0044
081102365	1.728	0.231	0.0258	0.0100	0.0165
081105614	1.280	1.368	0.0306	0.0147	0.0282
081107321	1.664	0.234	0.0504	0.0129	0.0173
081216531	0.768	0.429	0.0138	0.0037	0.0050
090108020	0.704	0.143	0.0241	0.0064	0.0088
090206620	0.320	0.143	0.0143	0.0063	0.0112
090227772	1.280	1.026	0.0053	0.0009	0.0011
090228204	0.448	0.143	0.0028	0.0005	0.0005
090308734	1.664	0.286	0.0120	0.0040	0.0059
090429753	0.640	0.466	0.0285	0.0115	0.0193
090510016	0.960	0.138	0.0049	0.0009	0.0011
100117879	0.256	0.834	0.0331	0.0122	0.0192

a chi-squared test on the white-noise signal power coefficients and rejecting any GRB that fails.

In summary, 1000 simulated light curves were generated and background noise was added. The light curves with background noise were then denoised using the same algorithm applied to actual GRB data in which preburst data were used as a surrogate for background. The simulated background-subtracted variances were then compared to the variances of the ideal light curves, i.e. light curves without external background noise. Signal-to-noise effects on the reliability of the method were also considered and found either to be small compared to our quoted errors or large enough that τ_β could not be determined. In the case of the latter the GRB was removed from the analysis. The results indicate that the background subtraction method is robust and gives confidence that external background noise can be subtracted from the GRB light curves with the assumption that preburst data can serve as a surrogate for background noise.

4.3 Selection criteria

We analysed 122 GRBs (61 long and 61 short) listed in the *Fermi* GBM-Burst Catalogue (Paciesas et al. 2012) for the first two years of the GBM mission. As discussed in Section 4.2, the signal-to-background ratio is a factor to be considered in recovering the intrinsic light curve (see equation 12). We required the following condition on the ratio of variances,

$$\frac{\beta_j^{\text{preburst}}}{\beta_j^{\text{burst}}} < 0.75, \tag{17}$$

for one or more octaves, j. In addition, we also required that the first-order polynomial fits to the noise region and to the scaling region each had a χ^2/d.o.f. that was less than 2. This reduced the sample to 14 short GRBs (Table 1) and 46 long GRBs (Table 2) for a total of 60, and it is these GRBs which are used to create Figs 4, 5 and 8. For boosting into the source frame (Figs 6 and 7) a known z is obviously required and this cut further reduced the data set to two short GRBs and 16 long GRBs for a total of 18 GRBs considered in the source frame (see Table 3).

5 RESULTS AND DISCUSSION

For a large sample of short- and long-GBM bursts, we have used a technique based on wavelets to determine the minimum time-scale (τ_β) at which scaling processes dominate random noise processes.

Table 2. Long GRBs (observer frame).

GRB	T_{90} (s)	δT_{90} (s)	τ_β (s)	$\delta\tau_\beta^-$ (s)	$\delta\tau_\beta^+$ (s)
080723557	58.369	1.985	0.0440	0.0113	0.0151
080723985	42.817	0.659	0.1894	0.0557	0.0789
080724401	379.397	2.202	0.0741	0.0208	0.0290
080804972	24.704	1.460	0.4306	0.1336	0.1937
080806896	75.777	4.185	0.4189	0.1471	0.2268
080807993	19.072	0.181	0.0232	0.0096	0.0164
080810549	107.457	15.413	0.1353	0.0648	0.1243
080816503	64.769	1.810	0.1067	0.0428	0.0715
080817161	60.289	0.466	0.1919	0.0402	0.0509
080825593	20.992	0.231	0.0775	0.0138	0.0168
080906212	2.875	0.767	0.1011	0.0182	0.0222
080916009	62.977	0.810	0.2266	0.0630	0.0872
080925775	31.744	3.167	0.1748	0.0425	0.0562
081009140	41.345	0.264	0.1095	0.0170	0.0201
081101532	8.256	0.889	0.0948	0.0302	0.0444
081125496	9.280	0.607	0.2182	0.0504	0.0656
081129161	62.657	7.318	0.0912	0.0292	0.0429
081215784	5.568	0.143	0.0319	0.0043	0.0050
081221681	29.697	0.410	0.2701	0.0641	0.0841
081222204	18.880	2.318	0.1956	0.0533	0.0732
081224887	16.448	1.159	0.2055	0.0356	0.0431
090102122	26.624	0.810	0.0347	0.0111	0.0164
090131090	35.073	1.056	0.0733	0.0169	0.0220
090202347	12.608	0.345	0.1444	0.0575	0.0954
090323002	135.170	1.448	0.1598	0.0436	0.0599
090328401	61.697	1.810	0.0682	0.0139	0.0175
090411991	14.336	1.086	0.0673	0.0391	0.0935
090424592	14.144	0.264	0.0249	0.0031	0.0036
090425377	75.393	2.450	0.1346	0.0369	0.0508
090516137	118.018	4.028	0.4938	0.2063	0.3544
090516353	123.074	2.896	0.7992	0.5686	1.9711
090528516	79.041	1.088	0.1314	0.0320	0.0423
090618353	112.386	1.086	0.2631	0.0536	0.0673
090620400	13.568	0.724	0.1667	0.0422	0.0564
090626189	48.897	2.828	0.0498	0.0078	0.0093
090718762	23.744	0.802	0.1621	0.0482	0.0686
090809978	11.008	0.320	0.2436	0.0515	0.0652
090810659	123.458	1.747	0.7319	0.3027	0.5161
090829672	67.585	2.896	0.0678	0.0141	0.0177
090831317	39.424	0.572	0.0266	0.0103	0.0169
090902462	19.328	0.286	0.0223	0.0026	0.0029
090926181	13.760	0.286	0.0435	0.0061	0.0070
091003191	20.224	0.362	0.0300	0.0051	0.0062
091127976	8.701	0.571	0.0395	0.0059	0.0069
091208410	12.480	5.018	0.0621	0.0180	0.0254
100414097	26.497	2.073	0.0418	0.0074	0.0090

The τ_β is the intersection of the scaling region (red-noise) of the spectrum in the log-scale diagram with that of the flat portion representing the (white-noise) random noise component. This transition time-scale is the shortest resolvable variability time for physical processes intrinsic to the GRB. Histograms of the extracted τ_β values for long and short GRBs are shown in Fig. 4. We make two observations regarding these histograms: (1) there is a clear temporal offset in the extracted mean τ_β values for long and short GRBs. We believe this is the first clear demonstration of this temporal difference. Walker et al. (2000), who studied the temporal variability of long and short bursts using the BATSE data set, did not report a systematic difference between the two types of bursts. (2) The two histograms are quite broad and very similar in dispersion. While the difference in the mean τ_β is understandable (a point we discuss further elsewhere) the similarity of the dispersion is somewhat

Minimum Variability Time Scale, T_{90} (Observer Frame)
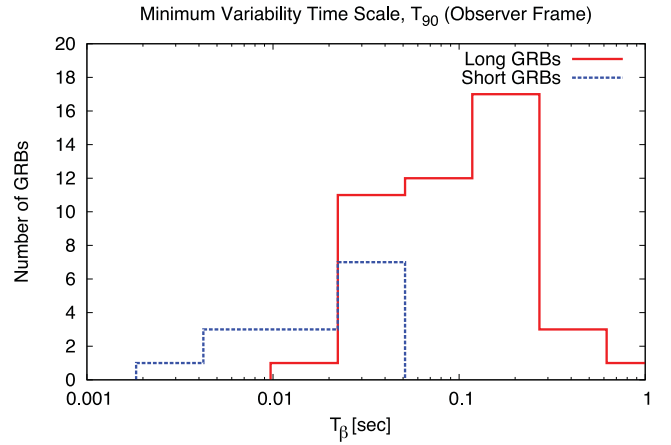
Figure 4. A histogram of minimum variability time-scales, in the observer frame, for long and short GRBs. It is clear that the distribution of long GRBs is displaced from the distribution of short GRBs.

T_{90} vs τ_β (Observer Frame)
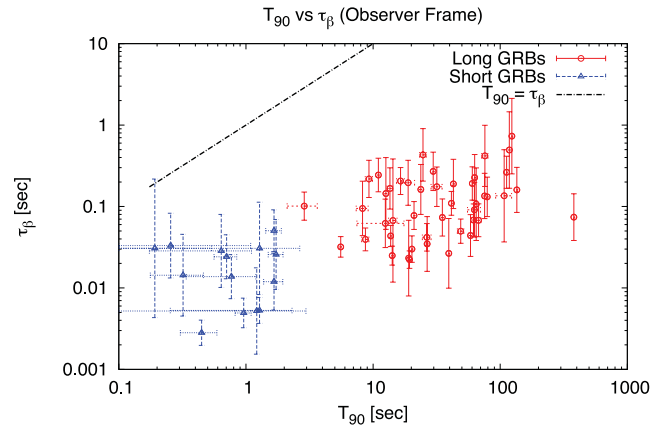
Figure 5. Minimum variability time-scale versus T_{90} in the observer frame.

T_{90} vs τ_β (Source Frame)
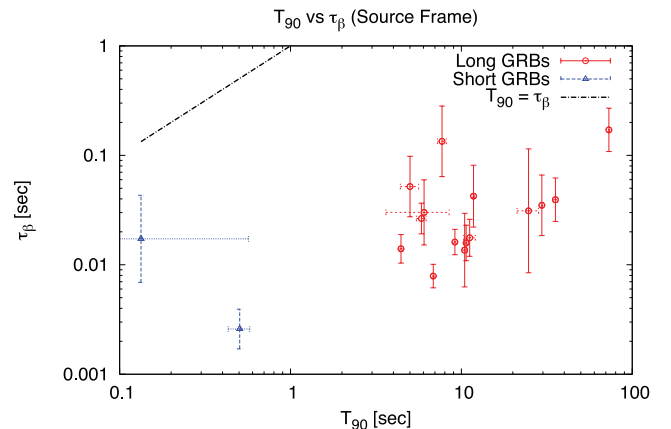
Figure 6. Minimum variability time-scale versus T_{90} in the source frame. The correction for time dilation shortens T_{90} and decreases the minimum variability time-scale of each burst.

surprising since the progenitors and the environment for the two types of bursts are presumably very different. The comparison is qualitative at best however because the τ_β scale has not been corrected for redshift (z), an effect that impacts the long bursts more than the short bursts. In passing, we note that
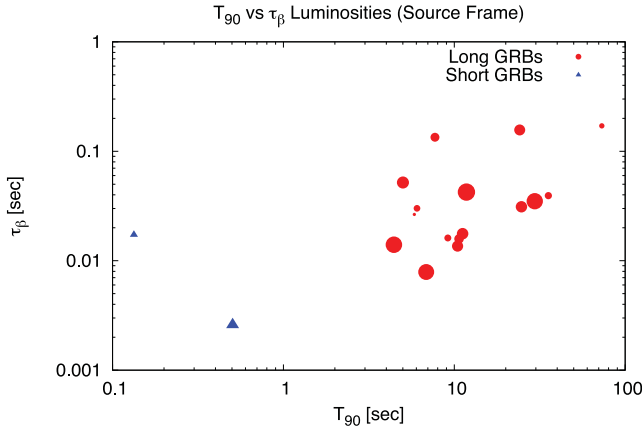
Figure 7. Minimum variability time-scale versus T_{90} with symbol size determined by luminosity (larger symbols for higher luminosity). No obvious relation between minimum variability time-scale and luminosity is apparent. See Fig. 6 for error bars.

the dispersion of the τ_β histogram (for long bursts) is in agreement with the results of Ukwatta et al. (2011), who performed a power density spectral analysis of a large sample of Swift long GRBs. In that work, the authors extracted threshold frequencies and related them to a variability scale.

In Fig. 5, we show a log–log plot of τ_β versus T_{90} (the duration of the bursts); long GRBs are indicated by circles, the short ones by squares and both time-scales are with respect to the observer frame. As in the histograms above, the fact that short GRBs, in general, tend to have smaller τ_β values compared to long GRBs is evident in this figure. Also shown in the figure (as a dash line) is the trajectory of τ_β equal to T_{90}. As we expect, no long GRBs exhibit a τ_β longer than T_{90} although interestingly a few short GRBs of extremely short

duration appear to be approaching the limit of equality. In addition to establishing a characteristic time-scale for short and long bursts, this figure also hints at a positive correlation between this time and the duration of bursts. We note that the τ_β scale spans approximately two decades for both sets of GRBs and that the two groups are fairly well clustered in the τ_β–T_{90} plane. A closer examination of the two groups, however, indicates that a correlation between τ_β and T_{90}, if present, is marginal at best. This is certainly true for the short-GRB group, especially given the large uncertainties in the T_{90}s for these bursts. The situation for the long-burst group on the other hand is not immediately clear. In order to explore this further, we cast the τ_β and the T_{90} time-scales into the source frame by applying the appropriate $(1 + z)$ factor to the GRBs for which the z is known. Unfortunately, the z is not available for the majority of the short GRBs, but we note that the correction is the same for both axes and is, to first order, small for the short GRBs since the mean z for this group is <0.8. The corrected results for long GRBs are shown as a log–log plot in Fig. 6. We see from this figure (and Fig. 5) the appearance of a very intriguing feature: a plateau region in which the τ_β is essentially independent of T_{90} and a scaling region in which τ_β appears to increase with T_{90}, with the transition occurring around T_{90} of the order of a few seconds.

If one assumes a positive correlation between luminosity and variability as suggested by a number of authors, then one might expect smaller τ_β values for higher luminosity bursts compared to those of lower luminosity. To investigate this, the data (in Fig. 6) are replotted in Fig. 7, in which the size of each datum symbol has been modulated by the gamma-ray luminosity of the burst, i.e. a large symbol implies a high luminosity and a small symbol a low luminosity. We see from Fig. 7 that no obvious connection between τ_β and luminosity is evident.

Under the assumption that τ_β is a measure proportional to the smallest causally connected structure associated with a GRB light

Table 3. Long and short GRBs (T_{90} and τ_β in observer frame). Luminosities are taken from references given in footnotes.

GRB	z	T_{90} (s)	δT_{90} (s)	τ_β (s)	$\delta\tau_\beta^-$ (s)	$\delta\tau_\beta^+$ (s)	L_{iso} (ergs s^{-1})	δL_{iso}^- (ergs s^{-1})	log δL_{iso}^+ (ergs s^{-1})
080804972	2.204	24.704	1.460	0.4306	0.1336	0.1937	[a]3.58×10^{52}	5.82×10^{51}	7.85×10^{51}
080810549	3.350	107.457	15.413	0.1353	0.0648	0.1243	[b]9.59×10^{52}	1.28×10^{52}	1.28×10^{52}
080916009	4.350	62.977	0.810	0.2266	0.0630	0.0872	[c]1.04×10^{54}	8.79×10^{52}	8.79×10^{52}
081222204	2.770	18.880	2.318	0.1956	0.0533	0.0732	[a]1.26×10^{53}	7×10^{51}	6×10^{51}
090102122	1.547	26.624	0.810	0.0347	0.0111	0.0164	[c]8.71×10^{52}	5.6×10^{51}	5.6×10^{51}
090323002	3.570	135.170	1.448	0.1598	0.0436	0.0599	[a]6.87×10^{53}	6.55×10^{53}	4.45×10^{52}
090328401	0.736	61.697	1.810	0.0682	0.0139	0.0175	[d]1.79×10^{52}	1.42×10^{51}	1.11×10^{51}
090424592	0.544	14.144	0.264	0.0249	0.0031	0.0036	[e]1.62×10^{52}	4×10^{50}	5×10^{50}
090510016	0.903	0.960	0.138	0.0049	0.0009	0.0011	[c]1.78×10^{53}	1.2×10^{51}	1.2×10^{51}
090516353	4.100	123.074	2.896	0.7992	0.5686	1.9711	[f]8.17×10^{52}	2.85×10^{52}	6.1×10^{51}
090618353	0.540	112.386	1.086	0.2631	0.0536	0.0673	[e]8.47×10^{51}	1.17×10^{51}	3.4×10^{50}
090902462	1.822	19.328	0.286	0.0223	0.0026	0.0029	[c]5.89×10^{53}	9.71×10^{51}	9.71×10^{51}
090926181	2.106	13.760	0.286	0.0435	0.0061	0.0070	[c]7.40×10^{53}	1.45×10^{52}	1.45×10^{52}
091003191	0.897	20.224	0.362	0.0300	0.0051	0.0062	[a]4.53×10^{52}	3.71×10^{51}	6.55×10^{51}
091127976	0.490	8.701	0.571	0.0395	0.0059	0.0069	[g]3.70×10^{51}	1.38×10^{50}	1.06×10^{50}
091208410	1.063	12.480	5.018	0.0621	0.0180	0.0254	[a]1.45×10^{52}	1.48×10^{51}	3.45×10^{51}
100117879	0.920	0.256	0.834	0.0331	0.0122	0.0192	[a]2.63×10^{52}	5.01×10^{51}	1.08×10^{52}
100414097	1.368	26.497	2.073	0.0418	0.0074	0.0090	[h]1.00×10^{53}	1.58×10^{52}	7.6×10^{51}

[a]Nava et al. (2011).
[b]GCN 8100.
[c]Ghirlanda et al. (2012).
[d]GCN 9057.
[e]Ukwatta et al. (2010).
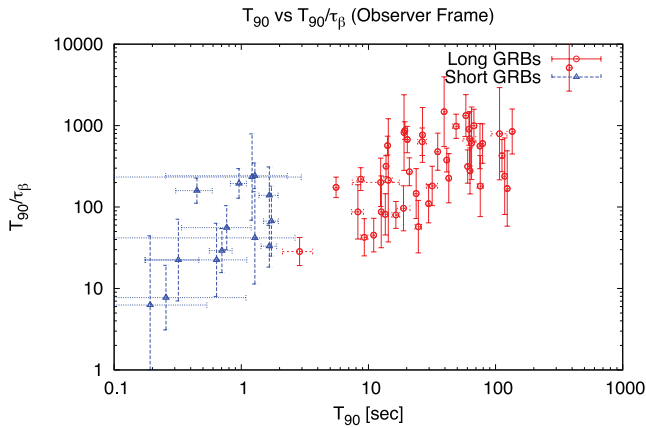[f]GCN 9415.
[g]GCN 10204.
[h]GCN 10595.

Figure 8. The ratio of duration-to-minimum variability time-scale (T_{90}/τ_β) versus T_{90}.

curve, it is then possible to interpret the scaling trend in terms of the internal shock model in which the basic units of emission are assumed to be pulses that are produced via the collision of relativistic shells emitted by the central engine. Indeed, we note that Quilligan et al. (2002) in their study of the brightest BATSE bursts with $T_{90} > 2$ s explicitly identified and fitted distinct pulses and demonstrated a strong positive correlation between the number of pulses and the duration of the burst. More recent studies (Hakkila & Cumbee 2008; Bhat & Guiriec 2011; Hakkila & Preece 2011; Bhat et al. 2012) provide further evidence for the pulse paradigm view of the prompt emission in GRBs. In our work, we have not relied on identifying distinct pulses but instead have used the multiresolution capacity of the wavelet technique to resolve the smallest temporal scale present in the prompt emission. If the smallest temporal scale is made from pulse emissions from the smallest structures, then we can get a measure of the number of pulses in a given burst through the ratio T_{90}/τ_β. In the simple model in which a pulse is produced every time two shells collide, then the ratio T_{90}/τ_β should show a correlation with the duration of the burst. A plot of this ratio versus T_{90} is shown for a sample of short and long bursts in Fig. 8. The correlation is apparent.

It is now widely accepted that the progenitors for the two classes of GRBs are quite distinct i.e. the merger of compact objects in the case of short GRBs and the collapse of rapidly rotating massive stars in the case of long GRBs. Formation of an accretion disc in the two cases is posed in a number of models, but important factors such as the size of the disc, the mass of the disc, the strength of the magnetic field, in addition to the magnitude of the accretion rate during the prompt phase, remain largely uncertain. With contributions from intrinsic variability of the central engine or nearby shock-wave interactions within a jet, we should not be surprised to observe a systematic difference in the extracted variability time-scales for long and short bursts, since the progenitors have different spatial scales. Knowing the variability time-scales, we can estimate the size of an assumed emission region. From Fig. 5, we note that the smallest temporal-variability scale for the short bursts is approximately 3 ms and that for the long bursts is approximately 30 ms. These times translate to emission scales of approximately 10^8 and 10^9 cm, respectively. Our variability times and size scales are generally consistent with the findings of Walker et al. (2000) although these authors also reported observing time-scales as small as a few microseconds. We find no evidence for variability times as low as a few microseconds.

Morsony et al. (2010) modelled the behaviour of a jet propagating through the progenitor and the surrounding circumstellar material and showed that the resulting light curves exhibited both short-term and long-term variability. They attribute the long-term variability, at the scale of a few seconds, to the interaction of the jet with the progenitor. They attribute the short-term scale, at the level of milliseconds, to the variation in the activity of the central engine itself. Alternatively, Zhang & Yan (2011) consider a model in which the prompt emission is the result of a magnetically powered outflow which is self-interacting and triggers rapid turbulent reconnections to power the observed GRBs. This model also predicts two variability components but interestingly and in contrast to the findings of Morsony et al. (2010), it is the slow component that is associated with the activity of the central engine, and the fast component is linked to relativistic magnetic turbulence. While we are not in a position to distinguish between these two models, it is intriguing nonetheless to note (see Fig. 5) that indeed there do appear to be two distinct time domains for the τ_β: a plateau region dominated primarily by short bursts although it includes some long bursts too, and a scaling region (i.e. a hint of a correlation between τ_β and T_{90}) that is comprised solely of long bursts. In addition, we observe that the time-scale in the plateau region is the order of milliseconds whereas that for the scaling region is approaching seconds.

There is considerable dispersion in the extracted τ_β. The variation is evident for both short- and long-duration GRBs. The main cause of this dispersion is not fully understood, but one factor that may play a significant role is angular momentum. As Lindner et al. (2010) note, the basic features of the prompt emission can be understood in terms of accretion that results via a simple ballistic infall of material from a rapidly rotating progenitor. Material with low angular momentum will radially accrete across the event horizon, whereas the material with sufficient angular momentum will tend to circularize outside the innermost stable circular orbit and form an accretion disc. Simulations that go beyond the simple radial infall model (Lindner et al. 2010, 2012) suggest that the formation of the disc leads to an accretion shock that traverses outwards through the infalling material. If one assumes that the initiation of such an accretion shock and the subsequent emission of the prompt gamma-rays are associated with a particular time-scale, the variability of this scale then (as given by the dispersion in τ_β for example) may reflect the different dynamics (initial angular momentum and the mass of the black hole) of each GRB in our sample. In the case of long GRBs, the mass of the central black hole can vary by an order of magnitude, thus potentially explaining a large part of the dispersion seen in the τ_β. However, a similar dispersion for short bursts is difficult to reconcile using the same arguments since the mass range for the central black hole in standard merger models (at least for NS–NS mergers) is expected to be significantly smaller.

6 CONCLUSIONS

We have studied the temporal properties of a sample of prompt-emission light curves for short- and long-duration GRBs detected by the *Fermi*/GBM mission. By using a technique based on wavelets, we have extracted the variability time-scales for these bursts. Our main results are summarized as follows.

(a) Both short- and long-duration bursts indicate a temporal variability at the level of a few milliseconds. Variability of this order appears to be a common feature of GRBs. This finding is consistent with the work of Walker et al. (2000). However, unlike these

authors we do not find evidence of variability at a time-scale of few microseconds.

(b) In general, the short-duration bursts have a variability time-scale that is significantly shorter than long-duration bursts. In addition, the τ_β values seem not to depend in any obvious way on the luminosity of the bursts. The dispersion over different GRBs in the extracted time-scale for short-duration bursts is an order of magnitude within the smallest variability time, that time being approximately 3 ms. The dispersion for the long-duration bursts is somewhat larger. The origin of the dispersion in either case is not known, although we should expect that the size of the initial angular momentum and the mass of the system play significant roles. We note in passing that the 3 ms time-scale may not be a physical lower limit and may be a result of signal to noise and the set of GRBs used in this analysis. We remind the reader that our light curve resolution was 200 μs, and if a strong enough signal within a range of time-scales between 0.5 and 3 ms were present, we would expect our technique to be sensitive to it.

(c) The ratio T_{90}/τ_β appears to be positively correlated with the minimum variability time-scale. This suggests further support for the pulse paradigm view of the prompt emission as being the result of shell collisions. In this respect, the minimum variability time-scale is likely related to key pulse parameters such as rise times and/or widths.

(d) For short-duration bursts, the variability parameter τ_β shows negligible dependence on the duration of the bursts (characterized by T_{90}). In contrast, the long-duration bursts indicate evidence for two variability time-scales: a plateau region (at the shortest time-scale) which is essentially independent of burst duration and a scaling region (at the higher time-scale) that shows a positive correlation with burst duration. The transition between the two regions occurs around T_{90} of the order of a few seconds in the source frame.

ACKNOWLEDGEMENTS

REFERENCES

Abry P., Flandrin P., Taqqu M. S., Veitch D., 2003, in Paul D., George O., Murad S. T., eds, Theory and Applications of Long-Range Dependence, Birkhauser, Boston, p. 527

Addison P. S., 2002, The Illustrated Wavelet Transform Handbook. IoP Publishing, Bristol

Anzolin G., Tamburini F., De Martino D., Bianchini A., 2002, A&A, 519, A69

Bhat P. N., Guiriec S., 2011, Bull. Astron. Soc. India, 39, 471

Bhat P. N. et al., 2012, ApJ, 744, 141

Coifman R. R., Donoho D. L., 1995, Translation-Invariant De-noising, Springer-Verlag, Berlin, p. 125

Fenimore E. E., Ramirez-Ruiz E., 2000, ApJ, 539, 712

Flandrin P., 1989, IEEE Trans. Inf. Theory, 35, 197

Flandrin P., 1992, IEEE Trans. Inf. Theory, 38, 910

Fritz T., Bruch A., 1998, A&A, 332, 586

Ghirlanda G., Nava L., Ghisellini G., Celotti A., Burlon D., Covino S., Melandri A., 2012, MNRAS, 420, 483

Hakkila J., Cumbee R. S., 2009, in Meegan C., Gehrels N., Kouveliotou C., eds, AIP Conf. Ser. Vol. 1133, Gamma-Ray Bursts: Sixth Huntsville Symposium. Am. Inst. Phys., New York, p. 379

Hakkila J., Preese R., 2011, ApJ, 740, 104

Howe D., Percival D., 1995, IEEE, Trans. Instrum. Meas., 44, 94

Kobayashi S., Piran T., Sari R., 1997, ApJ, 490, 92

Kostelich E. J., Schreiber T., 1993, Phys. Rev. E, 48, 1752

Kouveliotou C., Meegan C. A., Fishman G. J., Bhat N. P., Briggs M. S., Koshut T. M., Paciesas W. S., Pendleton G. N., 1993, ApJ, 413, L101

Lindner C. C., Milosavljevic M., Couch S. M., Kumar P., 2010, ApJ, 713, 800

Lindner C. C., Milosavljevic M., Shen R., Kumar P., 2012, ApJ, 750, 163

MacLachlan G. A., Shenoy A., Sonbas E., Dhuga K. S., Eskandarian A., Maximon L. C., Parke W. C., 2012, MNRAS, 425, L32

Mallat S. G., 1989, IEEE, Trans. Pattern Anal. Mach. Intell., 11, 674

Mandelbrot B. B., Van Ness J. W., 1968, SIAM Rev., 10, 422

Meegan C. et al., 2009, ApJ, 702, 791

Morsony B. J., Lazzati D., Begelman M. C., 2010, ApJ, 723, 267

Nava L., Ghirlanda G., Ghisellini G., Celotti A., 2011, A&A, 530, A21

Norris J. P., Bonnell J. T., Nemiroff J., Scargle J. D., Kouveliotou C., Paciesas W. S., Meegan C. A., Fishman G. J., 1995, ApJ, 439, 542

Paciesas W. S. et al., 2012, ApJ, 199, 18

Percival D. B., Walden A. T., 2002, Wavelet Methods for Time Series Analysis. Cambridge Univ. Press, Cambridge

Quilligan F., McBreen B., Hanlon L., McBreen S., Hurley K. J., Watson D., 2002, A&A, 385, 377

Ryde F., 2004, ApJ, 614, 827

Scargle J. D., 1982, ApJ, 263, 875

Sonbas E., MacLachlan G. A., Shenoy A., Dhuga K. S., Parke W. C., 2012, ApJ, preprint (arXiv:1210.6850)

Strang G., Nguyen T., 1997, Wavelets and Filter Banks. Wellesley-Cambridge Press, Wellesley

Tamburini F., De Martino D., Bianchini A., 2009, A&A, 502, 1

Ukwatta T. N. et al., 2010, ApJ, 711, 1073

Ukwatta T. et al., 2011, MNRAS, 412, 875

Walker K. C., Schaefer B. E., Fenimore E. E., 2000, ApJ, 537, 264

Zhang B., Yan H., 2011, ApJ, 726, 90

This paper has been typeset from a TEX/LATEX file prepared by the author.